Progress in Additive Manufacturing
https://doi.org/10.1007/s40964-024-00656-3

FULL RESEARCH ARTICLE

Geometry-induced process and part characteristics in support-free powder bed fusion of polypropylene at room temperature

Samuel Schlicht[1] · **Dietmar Drummer**[1]

Received: 29 April 2024 / Accepted: 7 May 2024

Abstract
Laser-based powder bed fusion (LPBF) of semi-crystalline polymers enables the support-free layer-wise manufacturing of geometrically diverse, complex components. In contrast to the established quasi-isothermal powder bed fusion of polymers at elevated temperatures, non-isothermal, cold processing strategies allow to significantly extend the range of applicable material systems. Relying on the superposition of discretized, fractal exposure strategies and the implicit mesoscopic compensation of crystallization shrinkage, the support-free LPBF of polypropylene at room temperature is demonstrated. The present paper displays the temporally and spatially discrete exposure of superposed fractal, space-filling curves that enable the support-free LPBF of polypropylene through combining the mesoscopic compensation of crystallization shrinkage and the laser-induced minimization of thermal shrinkage through the implementation of pre-exposure scans. The non-isothermal processing regime was observed to exhibit an intrinsic robustness towards the influence of processing parameters on emerging peak temperatures while showing a significant extent of accumulated heat within manufactured parts. Complementary mechanical characterizations showed an orientation-dependent influence of the applied energy density on emerging mechanical properties, correlated with geometry-dependent temporal process characteristics that implicitly influence the available coalescence time and the timespan available for the thermal homogenization.

Keywords Non-isothermal · Powder bed fusion · Laser sintering · Polypropylene · Support-free

1 Introduction and motivation

Powder bed fusion processes represent the established state of the art in small- and mid-scale metal- and polymer-based additive manufacturing processes of technical components. One significant advantage of polymer-based laser powder bed fusion processes is rooted in the inherently support-free processing, describing the support of manufactured parts through the surrounding powder. The support-free manufacturing in polymer-based powder bed fusion is enabled through the quasi-isothermal processing [1], describing the processing of polymer materials at elevated build chamber temperatures for slowing the crystallization of semi-crystalline polymers, minimizing crystallization-induced deflections. In contrast to polymer-based powder bed fusion processes, metal-based processes show a predominant dependency on the use of support structures arising from the rapid solidification of the melt, limiting the geometric freedom while increasing requirements regarding the post processing of parts, such as removing support structures. Combining the advantages of quasi-isothermal, support-free powder bed fusion of polymers with the rapid solidification furthermore embeds the potential for increasing the range of materials suitable for polymer-based powder bed fusion processes. Relying on the predominant application of polyamide 11 and polyamide 12 due to the high robustness toward process interruptions, curling, and warping, the technological potential of isothermal powder bed fusion processes is inherently limited.

✉ Samuel Schlicht
samuel.schlicht@fau.de

[1] Institute of Polymer Technology, Friedrich-Alexander-Universität Erlangen-Nürnberg, Am Weichselgarten 10, 91058 Erlangen, Germany

Published online: 17 May 2024

2 State of the art

2.1 Support-minimizing strategies in laser-based powder bed fusion

The application of support structures in laser-based additive manufacturing processes intends to minimize the occurrence of thermal and crystallization-induced deflections, arising from the layer wise manufacturing. Considering the labor-intensive removal of support structures and interlinked geometric limitations, recent developments address the quantitative reduction of required support-structures through geometric optimizations [2–4], optimized part orientations [5, 6] and exposure-based process optimizations through pulsed [7] and defocused laser beams [8]. Exceeding the mere minimization of supports, intrinsically support-free additive manufacturing necessitates the minimization of residual stresses, essential for avoiding part warping and increasing the overall process robustness. The optimization of residual stresses and the minimization of process-induced distortions were described through the application of segmented exposure strategies [9–11], allowing to reduce the distortion of manufactured parts in comparison to unsegmented exposure strategies, such as meander scanning. Representing a sophisticated, intrinsically scale-invariant approach to segmented exposure strategies, the application of fractal exposure strategies [12, 13], relying on employing fractal, self-similar, space-filling curves for exposing a particular cross section, allowing for reducing residual stresses while expanding the range of material suitable for laser-based additive manufacturing processes. Contrasting the described positive influence of segmented exposure strategies on the corresponding distortion, numerical findings have been described that show a partially negative influence of segmented strategies, however indicating a predominant influence of the applied laser power and the underlying scan speed [14].

Complementing the influences of applied exposure strategies on emerging residual stresses and distortions, geometry-induced temperature fields represent a fundamental limitation in laser-based manufacturing processes. Influenced by the thermal superposition of consecutive exposure scans, linear exposure strategies are intrinsically interlinked to geometry-dependent vector lengths and corresponding laser return times [15]. Demonstrated for laser-based processing [16] and electron beam melting [17, 18], the return time of the energy source embeds implications for emerging transient temperature fields, microstructural properties and the interlinked avoidance of process interruptions.

The established quasi-isothermal LPBF of polymers distinguishes itself through the intrinsically support-free manufacturing, characterized through the metastable, simultaneous occurrence of the polymer melt and surrounding powder [19–21]. Isothermal crystallization processes show a dependency of crystallization kinetics on the prevailing build chamber temperature [20, 22–26], allowing for a predominantly homogeneous crystallization of material systems with suitable crystallization kinetics. Relying on the slowed isothermal crystallization, a stable processing regime is enabled, minimizing deflection-induced process interruptions, hence constituting the foundation for the support-free processing. In contrast to quasi-isothermal processing strategies, non-isothermal processing varieties face challenging temporal boundary conditions arising from the considerably accelerated crystallization process [27, 28]. Without the implementation of compensation mechanisms or support structures, the layer wise, spatially inhomogeneous crystallization embeds the potential for the inhomogeneous contraction and balling of the polymer melt alongside considerable warping of the part through the crystallization-induced shrinkage of exposed layers [3]. Support-free manufacturing strategies, therefore, necessitate the implementation of mechanisms for compensating the crystallization-induced shrinkage as well as the subsequent thermal shrinkage of the solidified melt, minimizing the influence of micro- and mesoscale volumetric contractions on the overall part dimensions.

Combining aspects of the selective laser melting of metals and the support-free LPBF of polymers, recent developments demonstrate the feasibility of discretized exposure strategies for the support-free manufacturing of polyamide 12 [29, 30], polypropylene [31, 32] and polypropylene-polysaccharide composites [33]. Based on the application of fractal exposure paths, previously described for the minimization of stress cracking [12] and residual stresses [13] in powder bed fusion of metal alloys, the processing of polymers at ambient conditions below the crystallization temperature becomes feasible.

2.2 Transient thermal processing conditions in powder bed fusion of polymers

The thermal characteristics of the polymer melt obtained during the laser exposure embed significant implications for the stability of the process as well as microstructural, superficial, and mechanical characteristics of the manufactured component. Relying on the prevailing application of linear exposure strategies described in literature, linear thermal gradients are obtained from locally linear exposure strategies [16, 34, 35]. The segmentation of a particular cross-section allows for limiting the spatial expansion of a particular thermal gradient, influencing the formation of residual stresses in powder bed fusion of

metals [36–39]. The formation of linear thermal gradients is associated with the repetitive superposition of laser-induced temperature fields and the laser focus, leading to temperature fields with cross-section-specific characteristics [40–43]. Based on the interaction of the exposed cross-section and the applied exposure strategy, segmented as well as fractal exposure strategies were described to reduce the thermal variance arising from varying cross-sections. In particular, the application of fractal exposure strategies [44] is associated with intrinsically geometry-invariant exposure strategies as well as a significantly increased extent of heat diffusion [45]. Fractal exposure strategies, resembling fractal, space-filling curves [46], lead to the intrinsic formation of thermal gradients oriented in opposite directions [31], facilitating the rapid dissipation of heat and the minimization of thermal gradients across the exposed area. The geometry-variant properties, associated with the intrinsic self-similarity of fractal structures, was demonstrated for single exposure cycles [45]. Based on repetitive exposure cycles applied in non-isothermal processing strategies [32], an implicit influence of temporal process characteristics on the repetitive heating of a particular cross section emerges. The temporal discretization represents a fundamental prerequisite to the non-isothermal, support-free processing by enabling the solidification and shrinkage of molten material without compromising the macroscopic shape of the manufactured component. Hence, the influence of temporal as well as spatial characteristics need to be considered in discretized exposure processes, constituting a fundamental boundary condition.

3 Methodology

3.1 Discretized, superposed fractal exposure strategies

Exposure strategies, applied for the support-free, non-isothermal powder bed fusion of polypropylene encompass fractal, space-filling curves (*FASS curves*) [47, 48], characterized by their self-similar structure [49, 50]. Applying the Peano curve [51, 52] as a particular FASS curve, the exposure of any cross-section can be obtained applying an algorithm proposed by Yang et al. [44], that relies on the cropping of and alternating re-connection of cropped sections of the fractal curve. An intrinsic discretization of the exposure process is obtained through the four-fold superposition of the phase-shifted curves, enabling the discretized melting and subsequent crystallization by applying a significantly extended hatch spacing of 1.6 mm, corresponding to 320% of the laser focus diameter of $d_{\mathrm{Focus}} = 0.5$ mm ($I_{\mathrm{Focus}} = I_0/e^2$). The emerging exposure strategy is schematically displayed in Fig. 1. For stabilizing the non-isothermal part formation

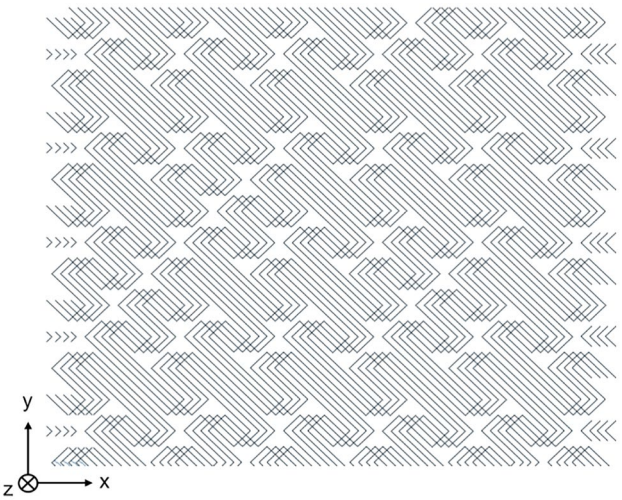

Fig. 1 Schematic depiction of a cutout of a fractal, discretized exposure strategy emerging from the four-fold superposition of closed, space-filling fractal Peano curves

through the preheating of upper, previously solidified layers, a preparation scan prior to the melting process is applied, relying on the dual consecutive meander exposure employing a hatch spacing of 0.7 mm, a laser power of $P = 20$ W and an exposure speed of 500 mm s^{-1}, yielding a predominantly homogeneous preheating through the application of an increased hatch spacing relative to quasi-isothermal, linear exposure strategies.

3.2 Machinery and process implementation

A freely configurable research system encompassing a high-speed galvanometer scanner (SCANLAB GmbH, Puchheim, Germany) and a pulse width modulated CO_2 laser ($\lambda = 10.6$ µm, Coherent, Inc., Santa Clara, USA) alongside a f-theta lens are applied for implementing the discretized, fractal exposure, obtaining a spot size of $d_{\mathrm{Focus}} = 0.5$ mm ($I_{\mathrm{Focus}} = I_0/e^2$) of the Gaussian intensity distribution [31]. For minimizing adverse effects of the powder coating process on the positioning accuracy of unsupported, solidified parts, a counter-rotating roller is employed, minimizing emerging shear stresses arising from the powder coating process. A layer height of 0.1 mm is kept constant throughout the processing.

3.3 Design of experiments

For characterizing the influence of support-free, non-isothermal processing strategies, tensile bars of type 1A (ISO 3167 [53]) are applied as underlying geometries for all manufacturing steps. Relying on the processing of commercially available polypropylene of type Ultrasint PP

1400 (BASF SE, Ludwigshafen, Germany), a full-factorial variation of the orientation of manufactured specimens in two orientations and of the applied laser power, varied in three steps, is conducted. The orientation of the specimen is varied in discrete angles of 45° and 30° relative to the powder bed surface, with an angle of 90° describing a vertical orientation of manufactured tensile bars. The underlying laser power is varied in steps of 24 W, 26 W, and 28 W while maintaining a constant area scan rate of 160 $mm^2\ s^{-1}$.

The position of manufactured specimens is varied in discrete angles of 30° and 45° relative to the powder bed, implicitly varying the exposed cross-section. In dependence on the applied angle, the projected surface of the part relative to the powder bed is implicitly varied, displayed in Fig. 2. The temporal discretization of consecutive exposure cycles is ensured through the parallel exposure of four geometrically identical specimens, enabling the discretized cooling of consecutive scans.

3.4 Process and part characterization

For assessing the influence of applied parameters on emerging process-dependent thermal conditions, the thermographic in situ monitoring in employed. Employing an infrared camera of type IRCAM VELOX 1310 k SM, the powder bed is continuously monitored using a frame rate of 500 Hz and a material-specific emission coefficient of $\varepsilon = 0.805$ [31]. For characterizing the emergence of process- and orientation-dependent thermal equilibria, the process is monitored over a range of 250 layers. Derived thermal characteristics are derived from square measurement areas encompassing $1 \times 1\ mm^2$, located in the center of the exposed area.

Complementary mechanical characterizations are based on ISO 527–2, employing a universal testing machine of type Zwick 1465 (ZwickRoell GmbH & Co. KG, Ulm, Germany). A strain rate of 0.25 $mm\ s^{-1}$ and 1 $mm\ s^{-1}$ are employed for the characterization of the elastic modulus and the tensile properties, respectively. Corresponding analysis of obtained fracture surfaces was conducted using a scanning electron microscope of type Zeiss Gemini (Carl Zeiss Microscopy GmbH, Oberkochen, Germany), applying an acceleration voltage of 10 kV.

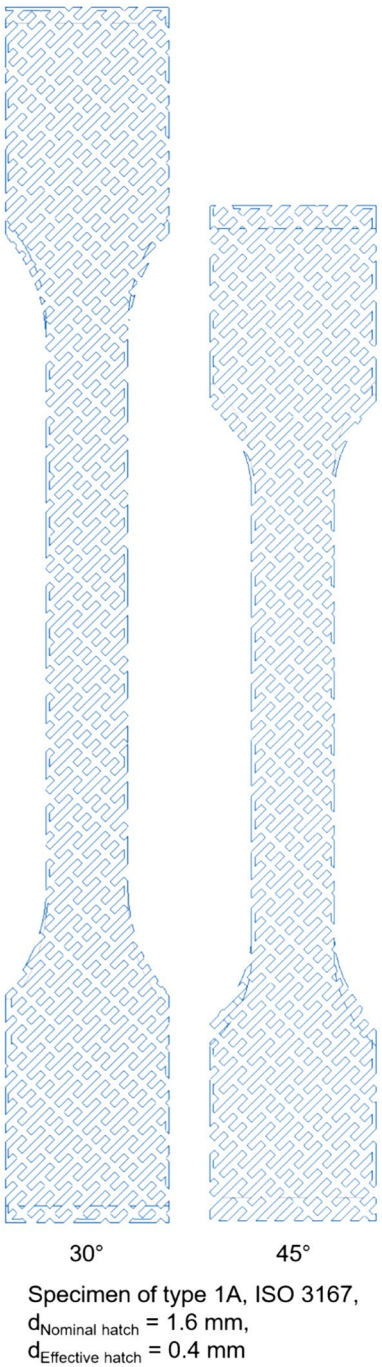

Fig. 2 Schematic depiction of orientation-specific exposure paths of a single exposure cycle; Accumulated depiction for all layers

4 Results and discussion

4.1 Process- and geometry-dependent transient processing conditions

Emerging from fundamentally different processing conditions in non-isothermal powder bed fusion processes, the discretized melting process and the intermediate cooling of the melt is associated with considerably increased cooling rates, influencing emerging peak temperatures as well as the part-specific thermal superposition and affected morphological and mechanical properties, previously described for laser-based PBF processes [41, 54] and electron beam melting [34] with linear exposure strategies. Relying on the

discretized exposure process, a step-wise energy input is correlated with the segmented increase of the superficial temperature of the exposed cross-section. Contrasting process characteristics observed in quasi-isothermal powder bed fusion, the thermal accumulation within the exposed layer does not depict a direct correlation with emerging peak temperatures, reflected in predominantly constant peak temperatures over a wide temporal range, evident in Fig. 3.

The non-linear influence of the applied laser power on emerging peak temperatures is assumed to rely on the exposure-induced coalescence of particles and the implicit adaption of thermal and optical properties of the exposed cross-section. In particular, the initial discretized exposure scan is associated with the highest peak temperatures, followed by a rapid quenching of the melt. In contrast to observed peak temperatures, subsequent exposure cycles lead to an increase in the equilibrium temperature and a slowed cooling of the surface. Underlying physical mechanisms are assumed to rely on the improved thermal conductivity of partially adhering material and an increased optical penetration depth, limiting the emergence of increased superficial peak temperatures. Similarly, no statistically significant influence of the applied laser power on emerging peak temperatures is observed within the applied processing window, displayed in Fig. 4.

Thermographic observations, therefore, display the exposure-induced variation of physical characteristics of the unfused powder that lead to an intrinsic robustness of emerging peak temperatures relative to changes of the applied process parameters. The influence of the part orientation is implicitly reflected in the temporal distance of the consecutive exposure cycles and the available time

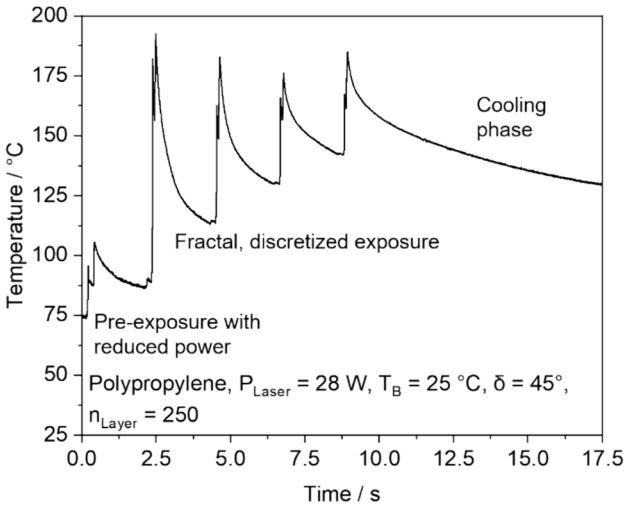

Fig. 3 Exemplary depiction of thermal characteristics of the exposure process obtained through a central point measurement of the cross section

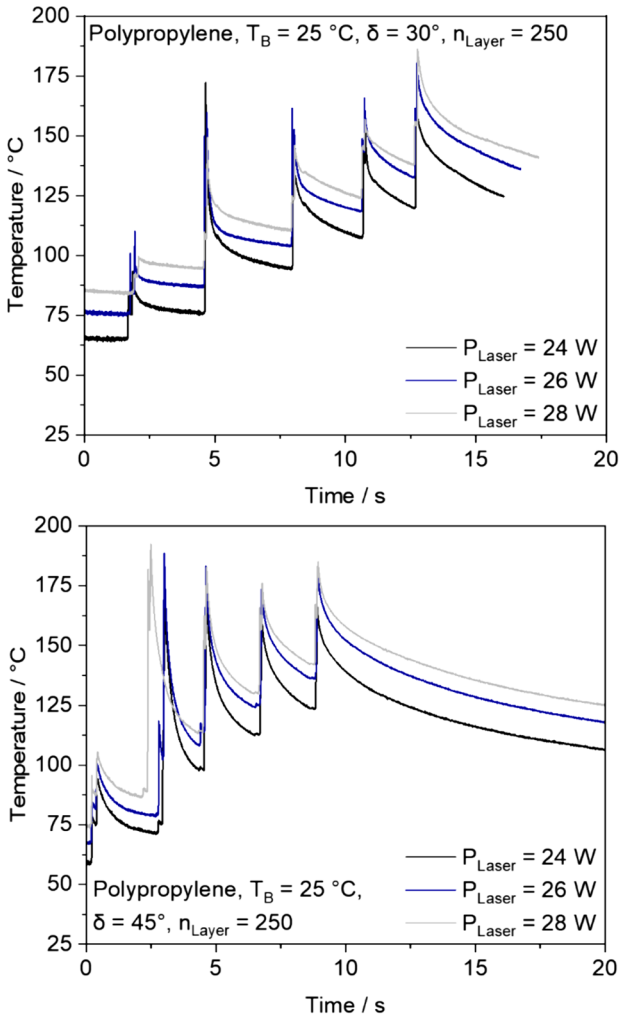

Fig. 4 Overview of parameter- and angle-dependent thermal characteristics, measured in the part center

for cooling, owing to the increased exposed area of each specimen. The intrinsic robustness of emerging peak temperatures is furthermore reflected in the invariance of emerging peak temperatures toward the layer-dependent buildup.

One significant thermal characteristic of non-isothermal processing manifests itself in the emerging equilibrium temperature, observed after each coating step. Following a particular layer, the part surface is cooled through the recoating of cold ($T = 25$ °C) polypropylene powder, shown in Fig. 5. Contrasting layer-dependent process dynamics observed for the quasi-isothermal powder bed fusion of semi-crystalline polymers [15], the emerging layer-wise buildup in non-isothermal processing depicts a layer-dependent increase of the equilibrium temperature, observed subsequent to the exposure process, displayed in Fig. 6. This phenomenon is likely associated with the predominant dissipation of heat through the solidified component, arising from the increased

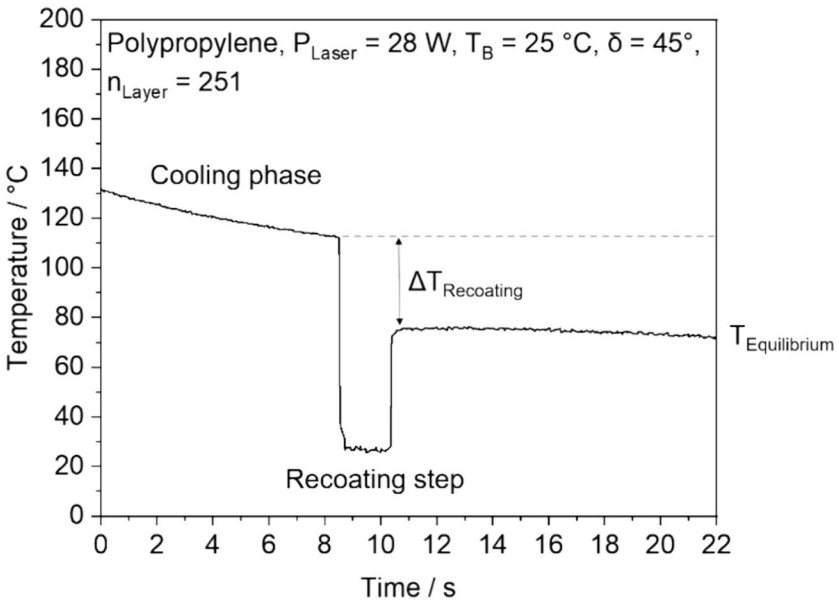

Fig. 5 Exemplary depiction of thermal characteristics of the recoating step, showing the coating-induced temperature difference and the emerging equilibrium temperature

thermal conductivity of the solidified, dense component. It, therefore, promotes the accumulation of thermal energy in the recrystallized component while inhibiting the dissipation of heat perpendicular to the build orientation due to insulating properties of unfused powder.

4.2 Process-induced mechanical characteristics

Independent on the applied part angle, the accumulation of thermal energy is observed when exceeding a number of $n = 10$ layers, followed by an angle-dependent increase over a range of 25 to 50 layers. An increasingly upwards orientation of the component contributes to the accelerated accumulation of heat, likely associated with the reduced surface-to-volume ratio of vertical components present at a reduced number of layers. The layer-dependent increase of observed temperatures indicates the emergence of part height-dependent crystallization kinetics, implicitly avoiding the formation of metastable modifications, observed for the manufacturing of thin components [31].

Arising from orientation- and process-dependent variations in the transient thermal processing conditions, a parameter-dependent elastic modulus, essential to design-related considerations, can be observed, shown in Fig. 7.

Derived process-dependent mechanical characteristics are predominantly influenced by the applied part orientation, depicting a negative orientation of the angle relative to the powder bed and the emerging tensile strength and the corresponding failure behavior. The orientation-dependent mechanical characteristics show slightly reduced values compared to an elastic modulus of 1250 MPa obtained in quasi-isothermal PBF and exhibit a significant, non-linear interaction with the applied laser power, displayed in Fig. 8. While specimens built applying an angle of 45° relative to the powder bed plane show a positive correlation of the applied laser power and the corresponding part stiffness, an increasing laser power is associated with a decreasing elastic modulus of specimens manufactured using an angle of 30°. The observed opposite influence of the applied laser powder is correlated with the divergence of orientation-dependent coalescence times, arising from the angle-dependent area of a particular cross-section, previously referred to in Fig. 4.

A reduced exposure timespan is associated with a reduced timespan available for the coalescence and the interlinked thermal homogenization through thermal conduction. Increased energy densities are assumed to facilitate the coalescence and the dense structure formation, promoting the densification of loose powder within a shorter timeframe. Considering a part angle of 30°, the exposure-induced reduction of the elastic modulus is correlated with morphological characteristics of manufactured parts, displayed in Fig. 9. The microscopically observed partial occurrence of spherical, likely degradation-induced pores [15] depicts a correlation with the aforementioned elastic modulus, reflecting the divergent influence of the laser power on parts manufactured under varying orientations. The nonlinear interaction of the laser power and the part angle indicates fundamentally varying mechanisms that govern the structure formation in non-isothermal processing. In particular, the influence of the equilibrium temperature and the interlinked control of the structure formation is of major importance for unifying all interlinked process mechanisms toward non-isothermal, geometry-invariant processing strategies at room temperature.

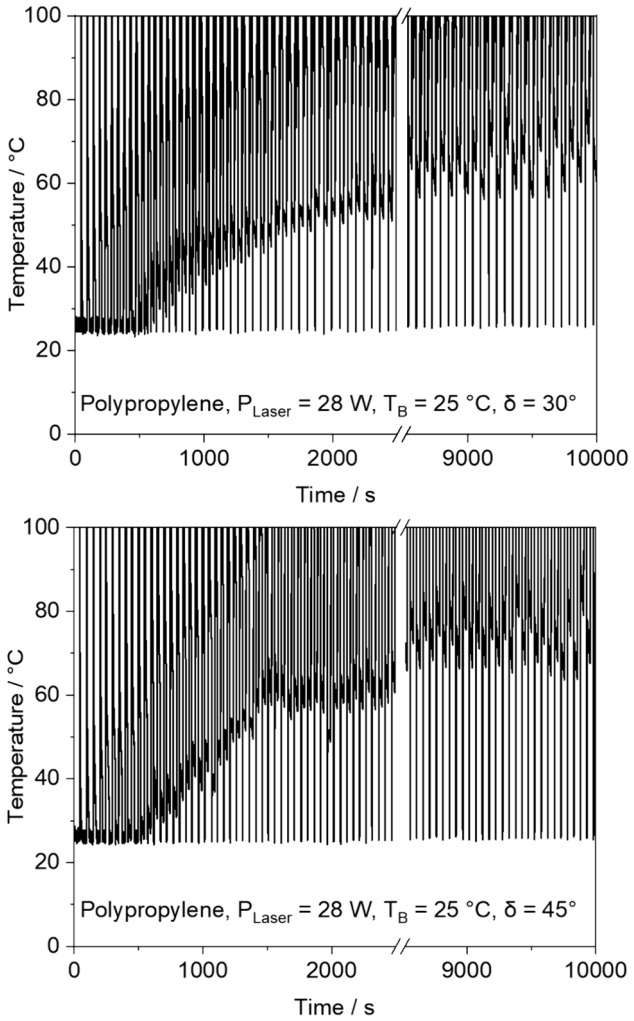

Fig. 6 Layer-dependent emerging temperatures with the visible thermal equilibrium temperatures after recoating in dependence on the part angle

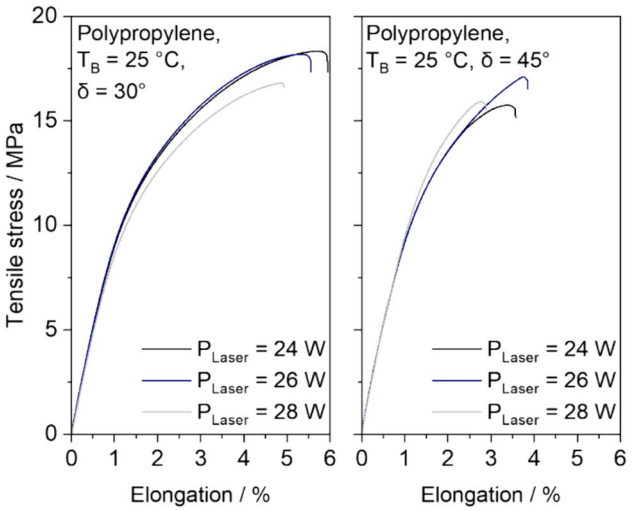

Fig. 7 Overview of orientation- and process-dependent strain–stress profiles

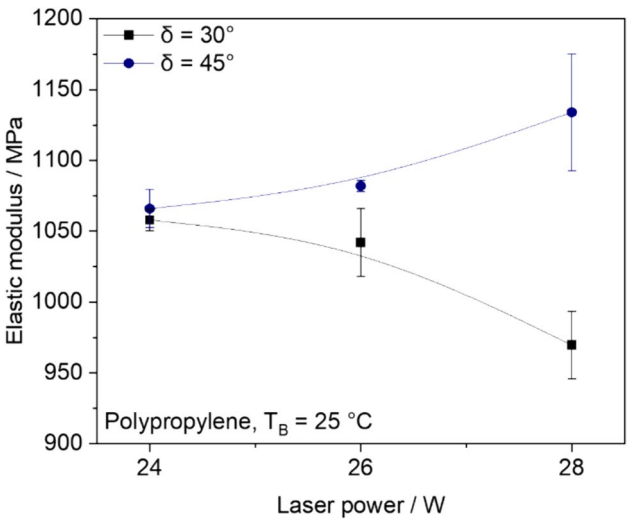

Fig. 8 Influence of the underlying laser power on the orientation-dependent elastic modulus, $n_{Specimen} = 5$

5 Conclusion and outlook

Combining the support-free properties of quasi-isothermal powder bed fusion of polymers with the cold processing regime of metal-based powder bed fusion embeds a variety of promising economical, ecological, and technological imperatives. These include, for instance, extending the applicable range of materials and significantly reducing the energy consumption of powder-based additive manufacturing processes. The temporally separated exposure of phase-shifted, fractal exposure strategies allows for the intrinsic avoidance of support structures. Contrasting quasi-isothermal processing strategies at elevated temperatures, a fundamentally divergent processing regime can be identified, associated with the orientation-adapted accumulation of thermal energy in manufactured parts. Furthermore, the influence of the part-specific cross-sectional area on the temporal distance of consecutive exposure cycles significantly affects the influence of the applied laser power on corresponding part properties. Hence, the influence of geometric boundary conditions is inherently interlinked to temporal process characteristics. Future research will address underlying geometry-dependent process mechanisms for minimizing geometry-induced part characteristics through the segmentation and the corresponding homogenization of the temporal discretization.

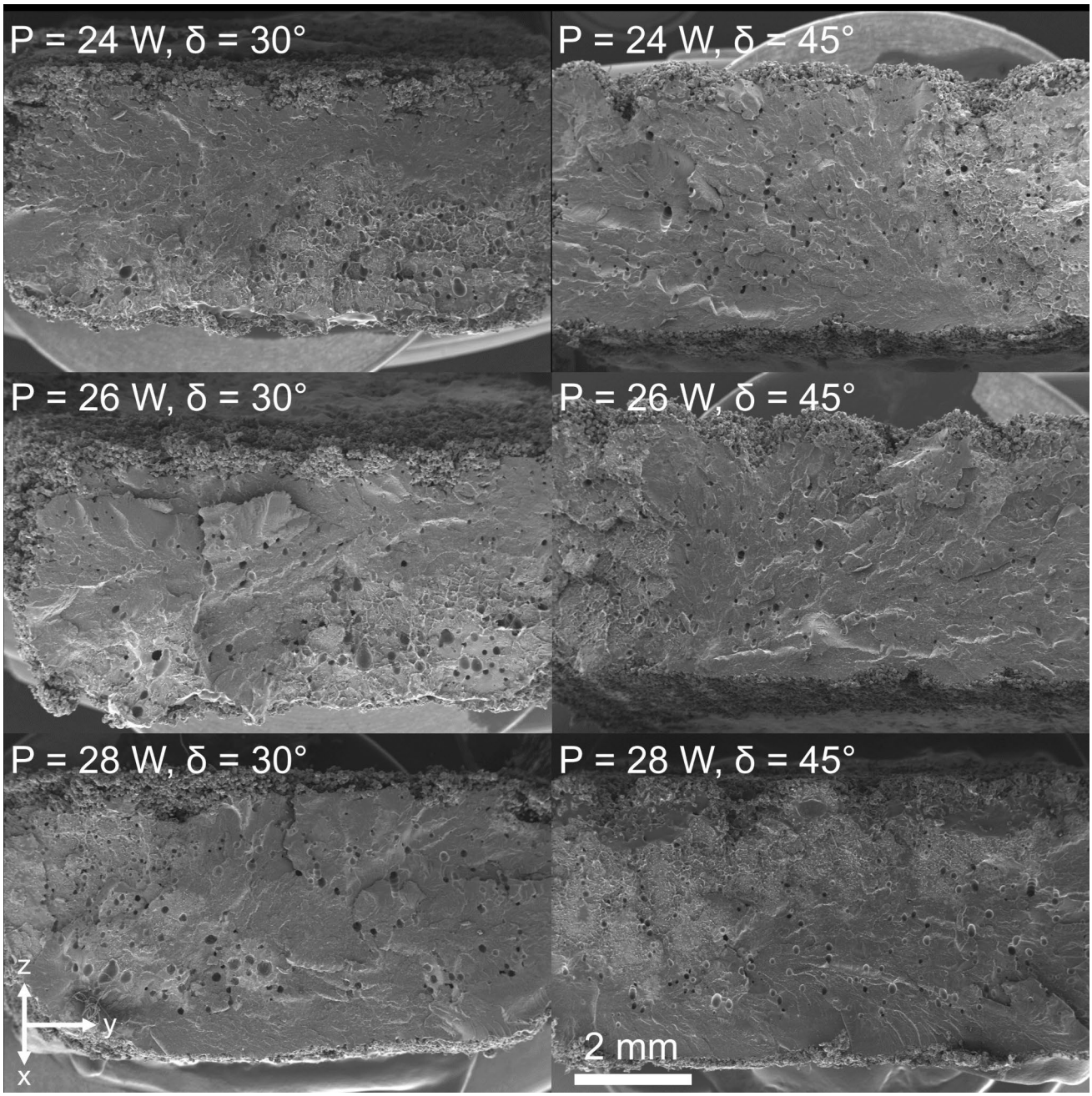

Fig. 9 Scanning electron micrographs of orientation- and process-dependent fracture surfaces

Acknowledgements Funded by the Deutsche Forschungsgemeinschaft (DFG, German Research Foundation) Project-ID 61375930 SFB 814–"Additive Manufacturing", subproject T10.

Author contributions Samuel Schlicht: conceptualization, methodology, software, validation, investigation, writing—original draft. Dietmar Drummer: supervision, project administration, funding acquisition.

Funding Open Access funding enabled and organized by Projekt DEAL.

References

1. Schmid M (2018) Laser sintering with plastics: technology, processes, and materials. Carl Hanser Verlag GmbH Co KG
2. Calignano F (2014) Design optimization of supports for overhanging structures in aluminum and titanium alloys by selective laser melting. Mater Des 64:203–213. https://doi.org/10.1016/j.matdes.2014.07.043
3. Gan MX, Wong CH (2016) Practical support structures for selective laser melting. J Mater Process Technol 238:474–484. https://doi.org/10.1016/j.jmatprotec.2016.08.006
4. Li Z, Zhang DZ, Dong P, Kucukkoc I (2017) A lightweight and support-free design method for selective laser melting. Int J Adv Manuf Technol 90:2943–2953. https://doi.org/10.1007/s00170-016-9509-0
5. Wang Y, Xia J, Luo Z et al (2020) Self-supporting topology optimization method for selective laser melting. Addit Manuf 36:101506. https://doi.org/10.1016/j.addma.2020.101506
6. Zhao J, Meng L, Lan X et al (2021) Design and experimental verification of self-supporting topologies for selective laser melting. Thin-Walled Struct 161:107419. https://doi.org/10.1016/j.tws.2020.107419
7. Grünewald J, Clarkson P, Salveson R et al (2021) Influence of pulsed exposure strategies on overhang structures in powder bed fusion of Ti6Al4V using laser beam. Metals (Basel). https://doi.org/10.3390/met11071125
8. Yuan Z, Chen X (2023) Novel approach for fabricating horizontal overhanging structures in selective laser melting. J Manuf Process 85:793–801. https://doi.org/10.1016/j.jmapro.2022.12.005
9. Yan X, Pang J, Jing Y (2019) Ultrasonic measurement of stress in SLM 316L stainless steel forming parts manufactured using different scanning strategies. Materials (Basel). 12:2719
10. Kruth J-P, Badrossamay M, Yasa E, et al (2010) Part and material properties in selective laser melting of metals. 16th Int Symp Electromachining, ISEM 2010
11. Tebaay LM, Hahn M, Tekkaya AE (2020) Distortion and dilution behavior for laser metal deposition onto thin sheet metals. Int J Precis Eng Manuf Technol 7:625–634. https://doi.org/10.1007/s40684-020-00203-9
12. Catchpole-Smith S, Aboulkhair N, Parry L et al (2017) Fractal scan strategies for selective laser melting of 'unweldable' nickel superalloys. Addit Manuf 15:113–122. https://doi.org/10.1016/j.addma.2017.02.002
13. Ma L, Bin H (2007) Temperature and stress analysis and simulation in fractal scanning-based laser sintering. Int J Adv Manuf Technol 34:898–903. https://doi.org/10.1007/s00170-006-0665-5
14. Şirin TB, Kaynak Y (2021) Prediction of residual stress and distortion in laser powder bed fusion additive manufacturing process of Inconel 718 alloy. Procedia CIRP 99:330–335. https://doi.org/10.1016/j.procir.2021.03.102
15. Greiner S (2023) Bedeutung der geometrieabhängigen Belichtungstemperaturen für das Lasersintern von Kunststoffen. Friedrich-Alexander-Universität Erlangen-Nürnberg (FAU)
16. Greiner S, Drummer D (2020) Infrared monitoring of modified hatching strategies for laser sintering of polymers. Proced CIRP 94:89–94. https://doi.org/10.1016/j.procir.2020.09.018
17. Breuning C, Markl M, Körner C (2023) A return time compensation scheme for complex geometries in electron beam powder bed fusion. Addit Manuf 76:103767. https://doi.org/10.1016/j.addma.2023.103767
18. Lei Y, Aoyagi K, Cui Y et al (2020) Process optimization and mechanical property investigation of non-weldable superalloy Alloy713ELC manufactured with selective electron beam melting. Mater Sci Eng A 787:139485. https://doi.org/10.1016/j.msea.2020.139485
19. Drummer D, Greiner S, Zhao M, Wudy K (2019) A novel approach for understanding laser sintering of polymers. Addit Manuf 27:379–388. https://doi.org/10.1016/j.addma.2019.03.012
20. Zhao M, Wudy K, Drummer D (2018) Crystallization kinetics of polyamide 12 during selective laser sintering. Polymers (Basel). https://doi.org/10.3390/polym10020168
21. Soldner D, Greiner S, Burkhardt C et al (2020) Numerical and experimental investigation of the isothermal assumption in selective laser sintering of PA12. Addit Manuf 37:101676
22. Ren M, Mo Z, Chen Q et al (2004) Crystallization kinetics and morphology of nylon 1212. Polymer (Guildf) 45:3511–3518. https://doi.org/10.1016/j.polymer.2004.03.027
23. Zhang R, Jariyavidyanont K, Du M et al (2022) Nucleation and crystallization kinetics of polyamide 12 investigated by fast scanning calorimetry. J Polym Sci 60:842–855. https://doi.org/10.1002/pol.20210813
24. Paolucci F, van Mook MJH, Govaert LE, Peters GWM (2019) Influence of post-condensation on the crystallization kinetics of PA12: From virgin to reused powder. Polymer (Guildf) 175:161–170. https://doi.org/10.1016/j.polymer.2019.05.009
25. Verkinderen O, Baeten D, Van Puyvelde P, Goderis B (2021) The crystallization of PA11, PA12, and their random copolymers at increasing supercooling: From eutectic segregation to mesomorphic solid solutions. Polym Cryst 4:e10216. https://doi.org/10.1002/pcr2.10216
26. Paolucci F, Baeten D, Roozemond PC et al (2018) Quantification of isothermal crystallization of polyamide 12: modelling of crystallization kinetics and phase composition. Polymer (Guildf) 155:187–198. https://doi.org/10.1016/j.polymer.2018.09.037
27. Alms J, Hopmann C, Wang J, Hohlweck T (2020) Non-isothermal crystallisation kinetics of polypropylene at high cooling rates and comparison to the continuous two-domain pvT model. Polymers (Basel) 12:1515. https://doi.org/10.3390/polym12071515
28. Schawe JEK (2015) Analysis of non-isothermal crystallization during cooling and reorganization during heating of isotactic polypropylene by fast scanning DSC. Thermochim Acta 603:85–93. https://doi.org/10.1016/j.tca.2014.11.006
29. Schlicht S, Greiner S, Drummer D (2022) Low temperature powder bed fusion of polymers by means of fractal quasi-simultaneous exposure strategies. Polymers (Basel). https://doi.org/10.3390/polym14071428
30. Schlicht S, Cholewa S, Drummer D (2023) Process-structure-property interdependencies in non-isothermal powder bed fusion of polyamide 12. J Manuf Mater Process. https://doi.org/10.3390/jmmp7010033
31. Schlicht S, Drummer D (2024) Accelerated non-isothermal powder bed fusion of polypropylene using superposed fractal exposure strategies. In: Drstvensek I, Pal S, Ihan Hren N (eds) Additive Manufacturing in Multidisciplinary Cooperation and Production. Springer International Publishing, Cham, pp 3–14
32. Schlicht S, Drummer D (2023) Thermal intra-layer interaction of discretized fractal exposure strategies in non-isothermal powder bed fusion of polypropylene. J Manuf Mater Process. https://doi.org/10.3390/jmmp7020063
33. Schlicht S, Drummer D (2024) Laser-based additive manufacturing of polypropylene-agarose composites: processing properties and compressive mechanical properties. In: AIP Conference Proceedings. American Institute of Physics, St. Gallen
34. Lee YS, Kirka MM, Dinwiddie RB et al (2018) Role of scan strategies on thermal gradient and solidification rate in electron beam powder bed fusion. Addit Manuf 22:516–527. https://doi.org/10.1016/j.addma.2018.04.038

35. Parry L, Ashcroft IA, Wildman RD (2016) Understanding the effect of laser scan strategy on residual stress in selective laser melting through thermo-mechanical simulation. Addit Manuf 12:1–15. https://doi.org/10.1016/j.addma.2016.05.014
36. Chen C, Yin J, Zhu H et al (2019) Effect of overlap rate and pattern on residual stress in selective laser melting. Int J Mach Tools Manuf 145:103433. https://doi.org/10.1016/j.ijmachtools.2019.103433
37. Cheng B, Shrestha S, Chou K (2016) Stress and deformation evaluations of scanning strategy effect in selective laser melting. Addit Manuf 12:240–251. https://doi.org/10.1016/j.addma.2016.05.007
38. Lu Y, Wu S, Gan Y et al (2015) Study on the microstructure, mechanical property and residual stress of SLM Inconel-718 alloy manufactured by differing island scanning strategy. Opt Laser Technol 75:197–206. https://doi.org/10.1016/j.optlastec.2015.07.009
39. Bagg SD, Sochalski-Kolbus LM, Bunn JR (2016) The effect of laser scan strategy on distortion and residual stresses of arches made with selective laser melting. In: American Society of Precision Engineering (ASPE) 2016 Summer Topical Meeting: Dimensional Accuracy and Surface Finish in Additive Manufacturing
40. Greiner S, Drummer D (2022) Understanding aspect ratio effects in laser powder bed fusion of polyamide 12 by means of infrared thermal imaging. Proced CIRP 111:253–256. https://doi.org/10.1016/j.procir.2022.08.060
41. Greiner S, Wudy K, Wörz A, Drummer D (2019) Thermographic investigation of laser-induced temperature fields in selective laser beam melting of polymers. Opt Laser Technol 109:569–576. https://doi.org/10.1016/j.optlastec.2018.08.010
42. Wegner A, Witt G (2011) Process monitoring in laser sintering using thermal imaging. 22nd Annu Int Solid Free Fabr Symp - An Addit Manuf Conf SFF 2011
43. Zhang W, Tong M, Harrison NM (2020) Scanning strategies effect on temperature, residual stress and deformation by multi-laser beam powder bed fusion manufacturing. Addit Manuf 36:101507. https://doi.org/10.1016/j.addma.2020.101507
44. Yang J, Bin H, Zhang X, Liu Z (2003) Fractal scanning path generation and control system for selective laser sintering (SLS). Int J Mach Tools Manuf 43:293–300. https://doi.org/10.1016/S0890-6955(02)00212-2
45. Greiner S, Schlicht S, Drummer D (2021) Temperature field homogenization by fractal exposure strategies in laser sintering of polymers. In: Proceedings of the 17th Rapid.Tech 3D Conference Erfurt, Germany, 22?23 June 2021. Carl Hanser Verlag GmbH & Co. KG, pp 188–197
46. Graf S (1987) Statistically self-similar fractals. Probab Theory Relat Fields 74:357–392. https://doi.org/10.1007/BF00699096
47. Bader M, Bungartz H-J, Mehl M (2011) Space-Filling Curves. In: Padua D (ed) Encyclopedia of Parallel Computing. Springer, US, Boston, MA, pp 1862–1867
48. Sagan H (2012) Space-filling curves. Springer Science & Business Media
49. Peitgen H-O, Jürgens H, Saupe D, et al (1992) Classical fractals and self-similarity. Chaos Fractals New Front Sci 63–134
50. Hutchinson J (1981) Fractals and self similarity. Indiana Univ Math J 30:713–747
51. Peano G (1890) Sur une courbe, qui remplit toute une aire plane. Math Ann 36:157–160
52. Musgrave K (1991) A Peano curve generation algorithm. In: Graphics Gems II. Elsevier, p 25
53. (2014) DIN EN ISO 3167:2014–11; Kunststoffe - Vielzweckprobekörper
54. Jain PK, Pandey PM, Rao PVM (2008) Effect of delay time on part strength in selective laser sintering. Int J Adv Manuf Technol 43:117. https://doi.org/10.1007/s00170-008-1682-3